Acta Crystallographica Section D
Biological Crystallography
ISSN 0907-4449

Structure of D-tyrosyl-tRNA^{Tyr} deacylase using home-source Cu *Kα* and moderate-quality iodide-SAD data: structural polymorphism and HEPES-bound enzyme states

Manickam Yogavel, Sameena Khan, Tarun Kumar Bhatt and Amit Sharma*

Structural and Computational Biology Group, International Centre for Genetic Engineering and Biotechnology, Aruna Asaf Ali Road, New Delhi 110 067, India

Correspondence e-mail: amit.icgeb@gmail.com

Received 10 November 2009
Accepted 15 February 2010

PDB References: D-tyrosyl-tRNA^{Tyr} deacylase, 3lmt; 3lmu; 3lmv.

D-Tyrosyl-tRNA^{Tyr} deacylase (DTD) is an editing enzyme that removes D-amino acids from mischarged tRNAs. The crystal structure of *Plasmodium falciparum* DTD (PfDTD) was determined using the iodide-SAD phasing method. Iodide-derivatized PfDTD crystals were obtained using the quick cryo-soaking procedure in which native crystals were soaked for a short period of 10–30 s in cryoprotectant solution containing 0.2–1 *M* NaI. Iodide-SAD data sets were collected to 3.3 and 2.74 Å resolution from PfDTD crystals that belonged to two different space groups, $P4_3$ and $P1$, using an in-house X-ray copper-anode source. This is the first report to detail structure solution using low iodide anomalous signal, modest resolution and redundancy and average solvent content for SAD phasing of 984 and 1312 amino acids in the triclinic $P1$ and tetragonal $P4_3$ space groups, respectively. A total of 85% and 56% of the residues were automatically built into the iodide-phased electron-density maps using *PHENIX AutoBuild*. The structure of HEPES-bound PfDTD was subsequently determined by molecular replacement and refined to 2.83 Å resolution. The crystals obtained from various batches of crystallization trials of PfDTD exhibited polymorphism in terms of belonging to different crystal forms and space groups. Even within a given crystal system the unit-cell parameters showed high non-isomorphism. These packing variations were exploited in order to conduct a systematic study of conformational changes in PfDTD. It is shown that the disposition of a ten-residue insertion loop affects packing within the PfDTD crystals and seems to determine the non-isomorphism in unit-cell parameters. By tracking the changes in PfDTD unit cells, it was possible to map conformational differences within PfDTD that may be of significance for enzyme activity.

1. Introduction

The occurrence of polymorphism in crystals of biological macromolecules is a common phenomenon as the behaviour of macromolecules in crystallization experiments is generally unpredictable. Crystals with different lattices or unit-cell parameters are sometimes observed in the same crystallization drop or in different crystallization conditions. In addition, non-isomorphism in protein crystals as a result of heavy-atom derivatization and cryocooling is also common and can be problematic. Many cases of the presence of non-isomorphism in protein crystals have been reported (Zhang *et al.*, 1995; Redinbo *et al.*, 1999; Verschueren *et al.*, 1999; Randal & Kossiakoff, 2000; Brodersen *et al.*, 2003). In a few cases, possible structural reasons that may trigger non-isomorphism have been reported, including studies on CysB (Verschueren *et al.*, 1999), human topoisomerase I (Redinbo *et al.*, 1999) and FabZ from *Plasmodium falciparum* (Swarnamukhi *et al.*, 2007).

D-Tyrosyl-tRNA^{Tyr} deacylase (DTD) is an editing enzyme that cleaves the ester bond between D-amino acids and tRNA. PfDTD shares some sequence identity (19–45%) to previously determined DTD structures from *Aquifex aeolicus*, *Escherichia coli* (Ferri-Fioni *et al.*, 2001), *Haemophilus influenzae* (Lim *et al.*, 2003), *Homo sapiens* (Kemp *et al.*, 2007) and *Leishmania major*. The dimeric PfDTD has a unique ten-residue insertion in the N-terminal region of the protein. We crystallized PfDTD in three different crystal forms: triclinic, monoclinic and tetragonal (Fig. 1). Initial screening of native PfDTD crystals for diffraction indicated medium-resolution diffraction (to lower than 3.5 Å resolution) and also extensive non-isomorphism in the unit-cell parameters. Further analysis showed that the triclinic unit cell was likely to contain six PfDTD molecules (three dimers), the asymmetric unit of the tetragonal form contained four dimers and the monoclinic crystal form contained three or six dimers in the asymmetric unit. Possible structure solutions obtained by the molecular-replacement (MR) phasing method using 3.5–3.0 Å resolution data were unconvincing. This may be a consequence of the ten-residue insertion loop in PfDTD or possibly of other small structural differences. We concurrently attempted the halide (iodide) quick cryo-soaking procedure for phase determination of PfDTD using previously published methods (Dauter *et al.*, 2000; Yogavel *et al.*, 2007, 2009). Here, we report the crystal structure of PfDTD determined using iodide-SAD data sets and the subsequent structure determination of HEPES-bound PfDTD (in which the HEPES was from the crystallization liquor) using the MR method. Analysis of the crystal packing shows that conformational changes in the unique insertion loop in PfDTD may play a major role in the non-isomorphism of the PfDTD crystals.

2. Materials and methods

2.1. Crystallization and preparation of iodide derivative

Crystallization of PfDTD was carried out at room temperature using the hanging-drop vapour-diffusion method by mixing 1 µl protein solution (5–10 mg ml^{-1} in 25 m*M* Tris–HCl pH 7.3, 100 m*M* NaCl) with 1 µl reservoir solution and equilibrating against 200 µl well liquor. Three different shapes (Fig. 1) of crystals were obtained using 0.1 *M* MES pH 6.2–6.8 or 0.1 *M* Tris–HEPES pH 7.5–8.5 and 25–30% PEG 3350 as the precipitant solution. Crystals were also obtained using 25% PEG 1500. In all cases PfDTD crystals were transferred to a cryoprotectant solution composed of a higher concentration of mother liquor for a short period (10–30 s) prior to freezing in a stream of cooled nitrogen gas. Halide-derivative PfDTD crystals were prepared by soaking native crystals for 10–30 s in cryoprotectant solution containing 0.2–1 *M* sodium iodide (NaI).

2.2. Data collection and processing

Data sets were collected at 100 K using Cu $K\alpha$ radiation ($\lambda = 1.54$ Å) on a MAR345 image-plate detector mounted on a Rigaku MicroMax-007 rotating-anode X-ray generator operated at 40 kV and 20 mA. A total of 360, 720 and 360 frames were collected in 1° oscillation steps with 300, 480 and 180 s exposures per frame for the data sets from PfDTD in space group $P4_3$ (PfDTD-$P4_3$), PfDTD in space group $P1$ (PfDTD-$P1$) and HEPES-bound PfDTD (PfDTD-HEPES), respectively. The crystal-to-detector distance was set to 300, 270 and 280 mm for PfDTD-$P4_3$, PfDTD-$P1$ and PfDTD-HEPES, respectively. The data sets were processed with the *HKL*-2000 program (Otwinowski & Minor, 1997) and relevant statistics are summarized in Table 1. For PfDTD-$P4_3$ and PfDTD-$P1$ Bijvoet mates were treated as equivalent reflections in scaling but were merged separately as I^+ and I^-.

2.3. Substructure solution, phasing, model building and refinement

Initially, the iodide-SAD anomalous signal was analyzed using *SHELXC* (Sheldrick *et al.*, 2001) and *SHELXD* (Sheldrick, 2008) in *HKL2MAP* (Pape & Schneider, 2004). A partial model was obtained by phase determination using

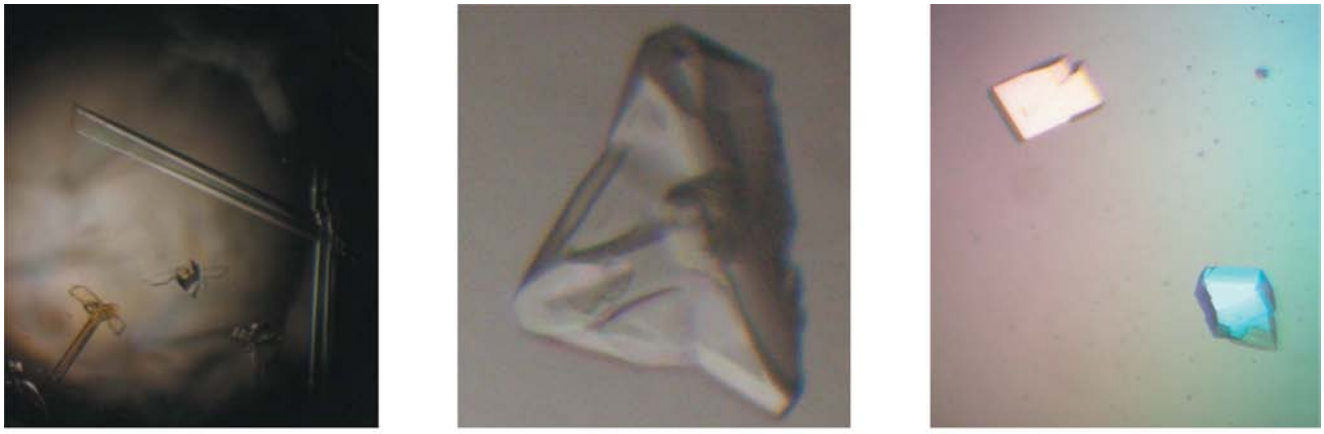

Figure 1
Three different morphologies of PfDTD crystals. Crystals were grown in (*a*) 0.1 *M* MES pH 6.2–6.5 and 25% PEG 3350 or 0.1 *M* Tris–HEPES pH 7.5–8.5 and 25% PEG 3350, (*b*) 25% PEG 1500 and (*c*) 0.1 *M* MES pH 6.8 and 25–30% PEG 3350.

Table 1
Summary of diffraction data and structure-refinement statistics.

Values in parentheses are for the highest resolution shell.

Data set	PfDTD-$P4_3$	PfDTD-$P1$	PfDTD-HEPES
PDB code	3lmu	3lmt	3lmv
Data collection			
Space group	$P4_3$	$P1$	$P1$
Unit-cell parameters (Å, °)	$a = b = 77.18$, $c = 214.52$, $\alpha = \beta = \gamma = 90$	$a = 55.34$, $b = 57.88$, $c = 91.63$, $\alpha = 102.8$, $\beta = 105.9$, $\gamma = 99.6$	$a = 51.65$, $b = 52.95$, $c = 89.68$, $\alpha = 75.4$, $\beta = 74.2$, $\gamma = 86.1$
Resolution range (Å)	50.0–3.30 (3.42–3.30)	50.0–2.74 (2.84–2.74)	50.0–2.82 (2.92–2.82)
Unique reflections	18914 (1869)	26067 (2375)	20391 (1702)
Completeness (%)	100 (100)	96.8 (89.1)	95.8 (79.5)
$\langle I\rangle/\langle\sigma(I)\rangle$	22.1 (6.6)	32.6 (6.4)	24.0 (4.6)
$R_{\rm merge}$	0.162 (0.516)	0.095 (0.364)	0.062 (0.313)
Multiplicity	14.9 (14.7)	8.0 (7.4)	3.9 (3.5)
Refinement			
Resolution range (Å)	32.0–3.30	50.0–2.75	50.0–2.83
Reflections in working set	17867	24336	19346
Reflections in test set	971	1304	1042
$R_{\rm work}/R_{\rm free}$ (%)	18.48/25.56	18.08/23.53	20.69/25.12
Model composition			
No. of protein residues	1186	928	881
Iodides/HEPES/SO_3	26 iodides	29 iodides	5 HEPES and 3 SO_3
Water molecules	—	177	—
Stereochemistry			
Bond lengths (Å)	0.01	0.01	0.01
Bond angles (°)	1.15	1.03	1.04
Ramachandran plot, residues in			
Most favoured regions (%)	82.2	86.5	89.4
Additional allowed regions (%)	16.3	11.8	9.8
Generously allowed regions (%)	0.9	1.1	0.4
Disallowed regions (%)	0.6	0.6	0.4
Mean B factors (Å^2)			
Protein atoms	47.6	39.0	60.0
Iodides/HEPES/SO_3	67.7	61.9	63.4/62.1
Water molecules	—	32.7	—
MolProbity			
MolProbity score	3.2	2.6	2.7
All-atom clash score	31.4	13.8	14.7
Bad rotamers (%/No. of residues)	7.4/60	5.2/39	7.1/55
Ramachandran favoured	87.7/1007	93.9/853	94.4/801
Ramachandran outliers	2.9/33	2.1/19	1.1/9

Table 2
Statistics of the anomalous signal-to-noise ratio [$\langle\Delta F/\sigma(\Delta F)\rangle$] *versus* resolution.

Values in bold indicate resolution bins with poor anomalous signal.

(*a*) PfDTD-*P*1.

Resolution	∞–8.0	8.0–6.0	6.0–5.0	5.0–4.2	4.2–4.0	4.0–3.8	3.8–3.6	3.6–3.4	3.4–3.2	3.2–3.0	3.0–2.75
360 frames											
No. of data	1075	1494	1859	3034	1160	1429	1721	2200	2744	3544	5725
$\langle I/\sigma(I)\rangle$	27.8	21.6	23.5	27.5	24.4	21.9	22.0	17.7	14.3	10.6	6.5
Completeness (%)	98.5	99.2	98.9	98.5	98.3	97.8	97.7	97.5	97.1	96.7	94.1
$\langle\Delta F/\sigma(\Delta F)\rangle$	1.49	1.68	1.56	1.44	1.35	**1.17**	**1.23**	**1.20**	**1.10**	**1.06**	**0.99**
720 frames											
No. of data	1081	1494	1870	3034	1162	1433	1724	2194	2752	3560	5763
$\langle I/\sigma(I)\rangle$	67.7	44.0	42.5	45.6	37.4	33.0	30.4	23.3	18.6	13.6	8.2
Completeness (%)	98.8	99.3	98.9	98.5	98.3	97.8	97.7	97.4	97.2	96.7	94.3
$\langle\Delta F/\sigma(\Delta F)\rangle$	3.03	2.83	2.38	2.01	1.75	1.49	1.46	1.34	**1.22**	**1.14**	**1.07**

(*b*) PfDTD-$P4_3$.

Resolution	∞–8.0	8.0–6.0	6.0–5.0	5.0–4.7	4.7–4.5	4.5–4.3	4.3–4.1	4.1–3.9	3.9–3.7	3.7–3.5	3.5–3.3
No. of data	1334	1806	2298	1111	899	1068	1321	1580	1949	2412	2091
$\langle I/\sigma(I)\rangle$	56.3	29.7	25.6	26.6	27.4	27.3	21.5	16.8	13.8	10.6	7.4
Completeness (%)	97.7	99.6	99.8	99.8	99.8	99.9	99.8	99.8	99.9	99.9	99.9
$\langle\Delta F/\sigma(\Delta F)\rangle$	3.32	2.27	1.64	1.52	1.33	**1.29**	**1.20**	**1.11**	**1.01**	**0.94**	**0.91**

PHENIX (Adams *et al.*, 2002) for PfDTD-$P4_3$ and PfDTD-*P*1. The PfDTD-HEPES structure was determined by the MR method using *MOLREP* (Vagin & Teplyakov, 1997) in the *CCP*4 suite (Collaborative Computational Project, Number 4, 1994) and with one PfDTD dimer as a starting model. The initial models were further completed by manual model building in *Coot* (Emsley & Cowtan, 2004) and were refined using *REFMAC*5 (Murshudov *et al.*, 1997) or *phenix.refine* (Adams *et al.*, 2002). The quality of all atomic models was assessed with *PROCHECK* (Laskowski *et al.*, 1993) and *MolProbity* (Chen *et al.*, 2010). Structural superpositions were carried out using *ALIGN* (Cohen, 1997) and figures were generated using *Chimera* (Pettersen *et al.*, 2004) and *PyMOL* (http://www.pymol.org).

3. Results and discussion

3.1. Structure determination of PfDTD-$P4_3$

Pyramid-shaped PfDTD crystals (Fig. 1*b*) were obtained using 25% PEG 1500 as a precipitant and these crystals belonged to the tetragonal space group $P4_3$ with four dimers in an asymmetric unit (solvent content ∼43%). Iodide derivatives were produced by soaking native crystals for a short period (10–30 s) in a cryoprotectant solution containing 500 m*M* NaI. Iodide-SAD data were collected to 3.3 Å resolution and the resulting mean anomalous signal-to-noise ratio [$|\Delta F|/\sigma(\Delta F)$] was 1.50. The anomalous signal was significant only to ∼4.5 Å resolution (Table 2). Substructure solution was successful using both *SHELXD* and *PHENIX* and most of the located iodide sites were identical using either program. Initially, eight iodide sites were located with *AutoSol* in *PHENIX* (Adams *et al.*, 2002)

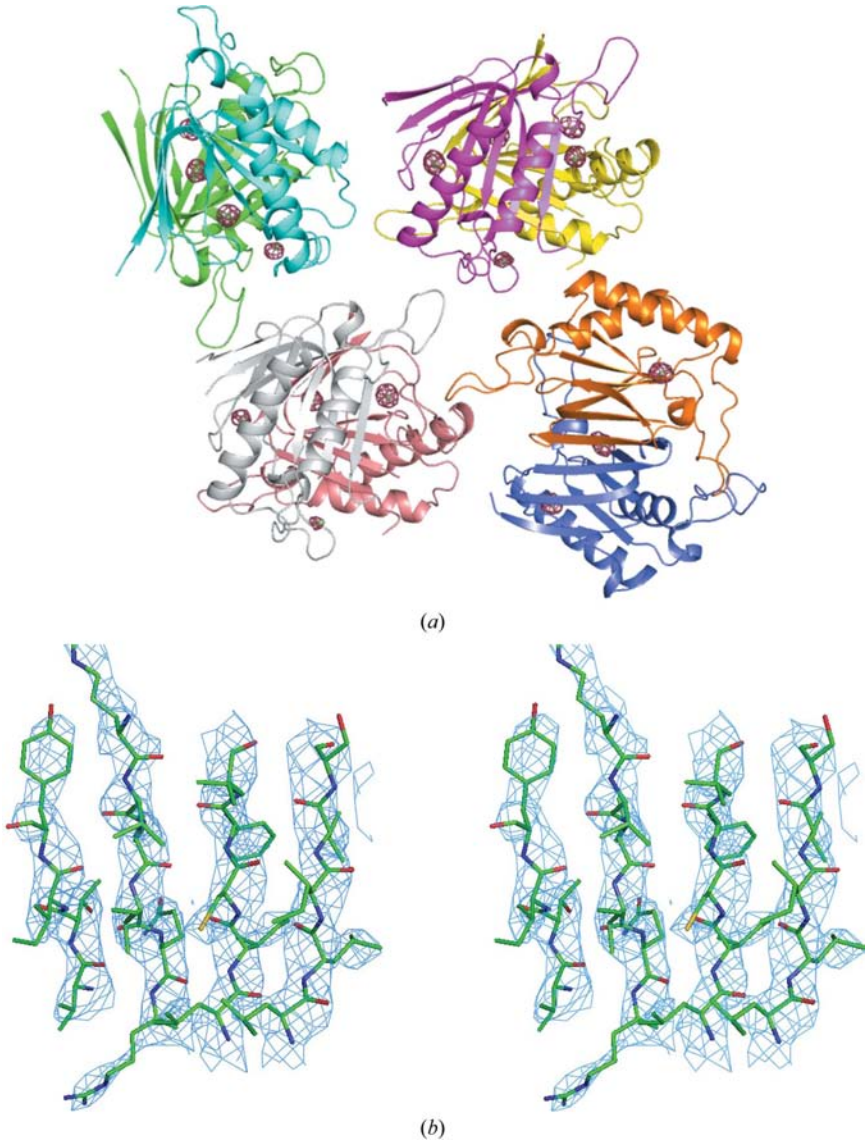

Figure 2
(*a*) Cartoon representation of PfDTD molecules in the asymmetric unit of PfDTD-$P4_3$. Anomalous difference electron density contoured at the 4σ level is shown together with bound iodides (magenta spheres). (*b*) Stereoview of representative regions of the electron-density map contoured at the 1.5σ level after density modification.

with an FOM of 0.37 and these sites were used for phasing. After phasing, a total of 16 sites were refined (Fig. 2*a*). The FOM increased to 0.75 on density modification and a preliminary model was built automatically. The obtained partial model was fed into *AutoBuild* for iterative model building and refinement. A total of 650 residues (65%) were built automatically and 430 side chains were placed with $R_{\rm work}$ and $R_{\rm free}$ values of 38% and 45%, respectively (Table 3). The experimental electron-density map obtained after density modification is shown in Fig. 2(*b*). The model was then subjected to a few rounds of noncrystallographic symmetry-restrained refinement. An additional 12 iodide sites were added and manual fitting of the amino-acid side chains into $2F_{\rm o} - F_{\rm c}$ and $F_{\rm o} - F_{\rm c}$ electron-density maps was performed. The electron density for the insertion-loop residues (17–26) and the C-terminal residues 160–164 was not clear and these portions were not included in the model refinement. Side-chain densities for some residues (such as Lys34, Asp68, Asn69, Lys70, Lys97, Lys100 and Lys125) were also not clear in the electron density and therefore are not modelled beyond the C^{β} atom.

3.2. Structure determination of PfDTD-*P*1

Iodide derivatives of PfDTD-*P*1 crystals were produced by soaking native plate-shaped crystals (Fig. 1*a*) for a short period (10–30 s) in a cryoprotectant solution containing 0.2–1 *M* NaI. Several crystals were tested and most of them diffracted to lower than 3.5 Å resolution with very poor anomalous signal and high non-isomorphism. Finally, successful iodide derivatization of PfDTD was achieved with a crystal that diffracted to 2.74 Å resolution which had been soaked in 1 *M* NaI for 10 s only. A total of 720 frames were collected from this crystal, which belonged to space group *P*1 with three dimers (984 amino acids) per unit cell and a solvent content of ∼49%. The mean anomalous signal-to-noise ratio [$|\Delta F|/\sigma(\Delta F)$] was 1.79 and the anomalous signal was only significant to ∼3.5 Å resolution (Table 2). Substructure solution was successful using both *SHELXD* and *PHENIX*. Initially, 17 anomalous scatters were located with *AutoSol* in *PHENIX* (Adams *et al.*, 2002) with an FOM of 0.46 and these sites were used for phasing. After phasing a total of 27 sites were refined (Fig. 3*a*) and after density modification the FOM increased to 0.75. A total of 843 residues (86%) were built automatically and 635 side chains were placed with $R_{\rm work}$ and $R_{\rm free}$ values of 26% and 31%, respectively (Table 3). The experimental electron-density map obtained after density modification is shown in Fig. 3(*b*). Subsequently, the model was subjected to a few rounds of noncrystallographic symmetry-restrained refinement. The residues in the two long loops (55–80 and 91–110) were not included in the NCS-restrained refinement. Two additional iodide sites were added and manual fitting of the amino-acid side chains was carried out in $2F_{\rm o} - F_{\rm c}$ and $F_{\rm o} - F_{\rm c}$ electron-density maps. Electron density for the insertion residues 17–26 was only clear in molecules *A* and *C* and therefore was not included in the final model. The C-terminal residues 161–164 were also disordered. The occupancy values of bound iodide ions were refined and ranged from 0.20 to 1.0. The final model of PfDTD-*P*1 included 928 residues, 29 iodide ions and 177 water molecules, with an $R_{\rm work}$ and $R_{\rm free}$ of 18.08% and 23.53%, respectively.

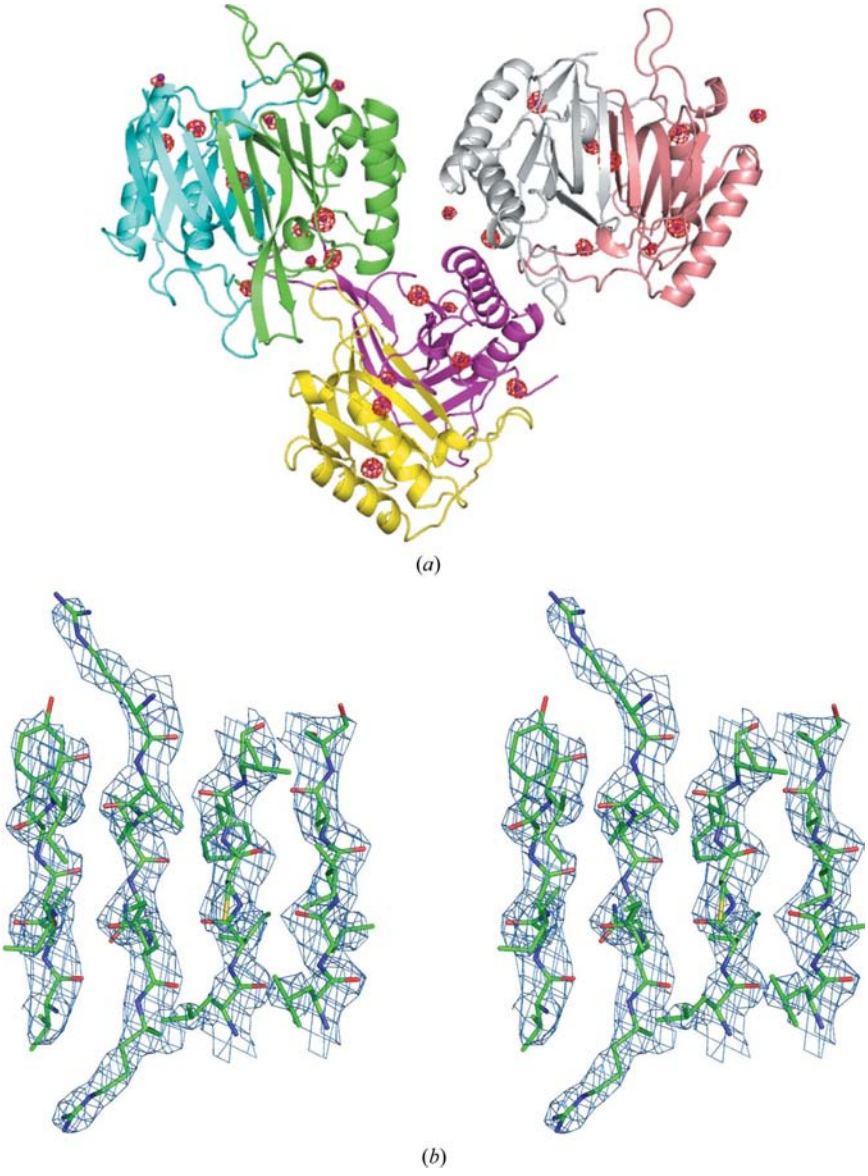

Figure 3
(*a*) Cartoon representation of PfDTD molecules in the unit cell of PfDTD-*P*1. Anomalous difference electron density contoured at the 5σ level is shown together with bound iodides (magenta spheres). (*b*) Stereoview of representative regions of the electron-density map contoured at the 1.5σ level after density modification.

3.3. Attempts to solve the PfDTD-*P*1 structure with a φ rotation range of 360° of data

The PfDTD-*P*1 structure was solved using *PHENIX* (Adams *et al.*, 2002) and a φ range of 720° (see Tables 1 and 2). These data had an average redundancy of ∼8 and a mean anomalous signal-to-noise ratio [$|\Delta F|/\sigma(\Delta F)$] of 1.79. To establish the effects of redundancy, the iodide data set was split into a φ range of 360° from the master data set of 720°. For the 360° data set the anomalous signal-to-noise ratio was 1.30 and the anomalous signal was weak (Table 2). The overall redundancy in the 360° data set was 3.9 (Table 2). Similarly, the overall $\langle I\rangle/(\langle\sigma(I)\rangle$ value for the 360° data set was 21.5, which is ∼0.66 times lower than that of the 760° data set (32.6). Substructure solution was attempted using *AutoSol* in *PHENIX*, but *HySS* failed to locate the iodides. Substructure solution in *SHELXD* was successful and 23 sites matched the iodide sites of the 760° data set. Phase calculations were carried out using *SHELXE* (Sheldrick, 2008) and *RESOLVE*, followed by attempts at model building using *AutoBuild* in *PHENIX* (Adams *et al.*, 2002) or *ARP*/*wARP* (Perrakis *et al.*, 2001). Both programs failed to build models for the 360° data set, although *SHELXD* was able to identify ∼23 iodide sites. It seems that the phases generated by both *SHELXE* and *RESOLVE* did not result in an interpretable electron-density map for automatic model building. This may be a consequence of the weak anomalous signal (Table 2) and modest resolution and redundancy with average solvent content and the 984 amino acids of the triclinic unit cell which needed to be phased.

3.4. Structure determination of PfDTD-HEPES

An initial model of PfDTD-HEPES was obtained by the MR method using *MOLREP* (Vagin & Teplyakov, 1997) because of the large unit-cell differences between the PfDTD-*P*1 and PfDTD-HEPES crystals. Following an initial round of rigid-body refinement, the structure was subjected to a few rounds of NCS-restrained refinement. The model was then manually inspected and some side chains were refitted using $2F_o - F_c$ and $F_o - F_c$ electron-density maps. During model building we discovered a bound HEPES molecule which was likely to have originated from the crystallization mother liquor. Inspection of difference Fourier maps revealed the presence of a strong peak (above 6σ) and a blob-like density at a distance of ∼3.5 Å from Ser87 in most molecules of PfDTD. In addition to this, two density blobs were found near Arg16 and Arg57 of molecule *B*. We interpreted these extra peaks as HEPES owing to the presence of 0.2 *M* HEPES in the crystallization buffer, but the fit of three of the piperazine rings of HEPES was unsatisfactory. We then replaced these with the sulfonic acid group SO_3, which fitted in a more satisfactory manner. Therefore, we were able to locate both intact HEPES and SO_3 groups bound to PfDTD. The final model of PfDTD-HEPES contained 881 residues, five HEPES molecules and three SO_3 groups.

3.5. Overall structure of PfDTD

PfDTD folds into the compact domain of the α/β class of proteins (Fig. 4*a*) and its structure is very similar to those of

the DTDs from *A. aeolicus*, *E. coli* (Ferri-Fioni *et al.*, 2001), *Haemophilus influenza* (Lim *et al.*, 2003), *Homo sapiens* (Kemp *et al.*, 2007) and *L. major*, with r.m.s.d.s in the range 1.1–1.9 Å. The PfDTD-*P*1 and PfDTD-HEPES crystals contain three independent dimeric molecules in the triclinic unit cell designated *AB*, *CD* and *EF*. The PfDTD-$P4_3$ crystals contain four dimers in the asymmetric unit designated *AB*, *CD*, *EF* and *GH*. In all cases, two or three of the PfDTD monomers have higher *B* values than the others in the various crystal forms. The r.m.s. deviations between monomers and dimers are in the ranges 0.3–1.2 and 0.4–1.5 Å, respectively. Relatively large r.m.s. deviations are observed in two long loop regions (residues 66–72 and 90–110). The *P. falciparum*-specific low-complexity insertion residues (17–26; KENIGENEKE; Fig. 4*b*) were not ordered in the PfDTD-$P4_3$ and PfDTD-HEPES structures, indicating flexibility. However, this insertion was found to be ordered in molecules *A* and *C* of the PfDTD-*P*1 structure. The insertion residues form an extended β-hairpin structure in one case and adopt a loop conformation in the other. These extra residues make no contacts with other parts of the PfDTD structure and are stabilized through lattice contacts only.

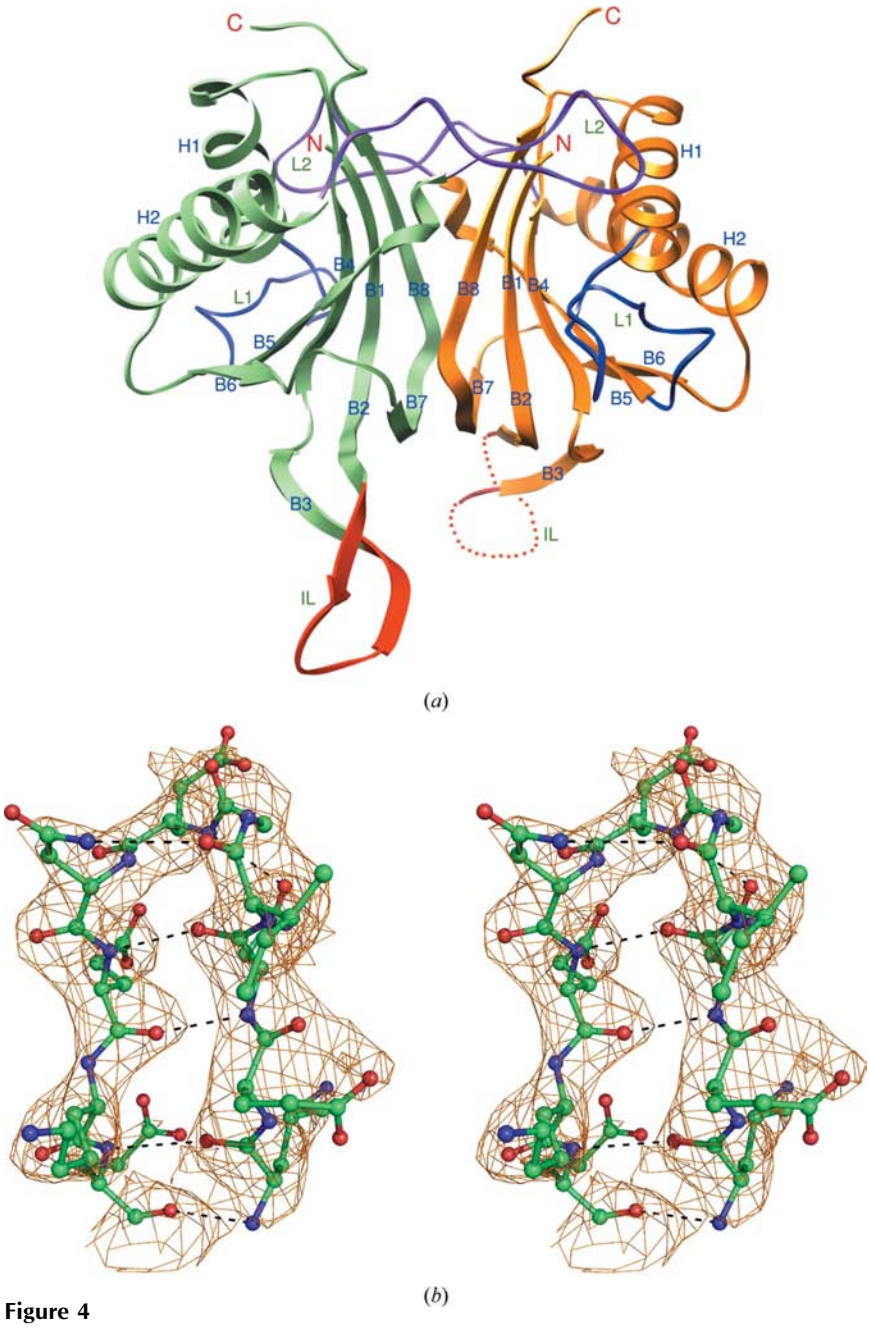

Figure 4
Overall structure of PfDTD. (*a*) Each monomer contains eight β-sheets (B1–B8), two α-helices (H1 and H2), two long loops (L1 and L2; blue and purple) and a low-complexity sequence insertion (IL; red). The disordered residues 17–26 in one monomer are marked with red dots. (*b*) Stereoview of ordered insertion residues and difference Fourier ($F_o - F_c$) map contoured at the 2.5σ level.

3.6. Bound iodides and their environments

A total of 29 iodides were found in the PfDTD-*P*1 structure and 26 were found in the PfDTD-$P4_3$ structure. Most of these bound iodides make conserved interactions with protein atoms and occupy the same positions within the six (*A*–*F*, PfDTD-*P*1) or eight (*A*–*H*, PfDTD-$P4_3$) PfDTD molecules (Fig. 5). Here, we discuss the bound iodides in PfDTD-*P*1 in detail. In general, the interaction distances between the iodides and protein atoms are in the range 3–4 Å. In many cases the interacting atoms are the side-chain N atoms of Arg, Lys and Asn residues. Some interactions involve the side-chain OH groups of Tyr and Ser residues and main-chain N atoms. Two tightly bound iodides (IOD1 and IOD2; Figs. 5*a* and 5*b*) were observed near the active site and in the dimer interface. These sites appeared first in the substructure solution and have high occupancy and lower *B* values; each makes several interactions with protein atoms. IOD1 makes four interactions with the OH group of Tyr116 and the N atoms of Gly135, Phe137 and Ser87 (Fig. 5*a*). The twofold-related dimer interface-bound IOD2 interacts with the side-chain atoms of Gln6 and Asn147 (Fig. 5*b*). The surface-bound iodides (IOD3–5) make one or two interactions with protein atoms as shown in Figs. 5(*c*)–5(*e*). The positions of the surface-bound iodides are not conserved and have displacements of 0.2–1 Å. IOD4 is located in the dimer-interface surface cavity formed by Arg57 of the reference molecule and Asn99 of the twofold-related molecule. Arg57 and Asn99 belong to two long loops (L1 and L2; Fig. 4*a*); these loops were not included in the NCS restraints during refinement. The displacement of IOD4 correlates with the movement of the side chains of Arg57 and Asn99.

Table 3
Substructure-solution, phasing and model-building statistics.

FOM, figure of merit. CC, correlation coefficient. SKEW, skew of the electron density in the map. CORR_RMS, the correlation of local r.m.s. density. FP, observed structure-factor amplitudes. FC, calculated structure-factor amplitudes.

	PfDTD-$P4_3$	PfDTD-$P1$
Bijvoet pairs	18412	24193
Mean anomalous signal ($\langle\Delta F\rangle/\langle F\rangle$)	0.089	0.076
Mean anomalous signal-to-noise ratio [$\langle\Delta F/\sigma(\Delta F)\rangle$]	1.50	1.79
AutoSol		
No. of sites	16	27
SKEW	0.16	0.16
CORR_RMS	0.77	0.83
FOM	0.37	0.46
Estimated map CC	0.34 ± 0.16	0.43 ± 0.27
After *DM*		
R factor (FC *versus* FP)	0.28	0.32
FOM	0.69	0.75
Map CC	0.65	0.61
AutoBuild		
Residues built	851	843
Side chains placed	430	635
R_{work}/R_{free}	0.38/0.45	0.26/0.31
Map CC	0.64	0.73
Final refinement statistics		
R_{work}/R_{free} (%)	18.48/25.56	18.08/23.53
No. of protein residues	1186	928

3.7. Bound HEPES and SO_3 molecules

Interestingly, regions near the active sites of molecules *A*–*D* of PfDTD-HEPES are occupied by HEPES molecules (Fig. 6*a*). In addition to this, HEPES was also found on the surface between molecule *B* and the symmetry-related molecule *C*. A weakly bound HEPES was observed near the active site of molecule *F* and was only modelled as a sulfonic acid group (SO_3), while the active site of molecule *E* is empty. Two weakly bound HEPES molecules were also found on either side of the insertion residues and were modelled as SO_3 groups. The bound HEPES molecules are stabilized by a number of interactions with protein residues at distances of 2.6–3.8 Å (Figs. 6*b*). The region around the PfDTD active site is positively charged in nature and a negatively charged sulfonic acid group of HEPES chelates here (Fig. 6*c*).

3.8. Loop structure and packing variations in non-isomorphic crystals of PfDTD

PfDTD crystallizes in three different space groups with different crystal shapes (Fig. 1). The same crystallization mother liquor yielded different crystal systems. A systematic analysis was performed on various triclinic forms (T1–T5) of PfDTD crystals (Table 4). The triclinic unit-cell parameters were in the range $a = 51 \pm 8$, $b = 53 \pm 5$, $c = 90 \pm 3$ Å, $\alpha = 102$

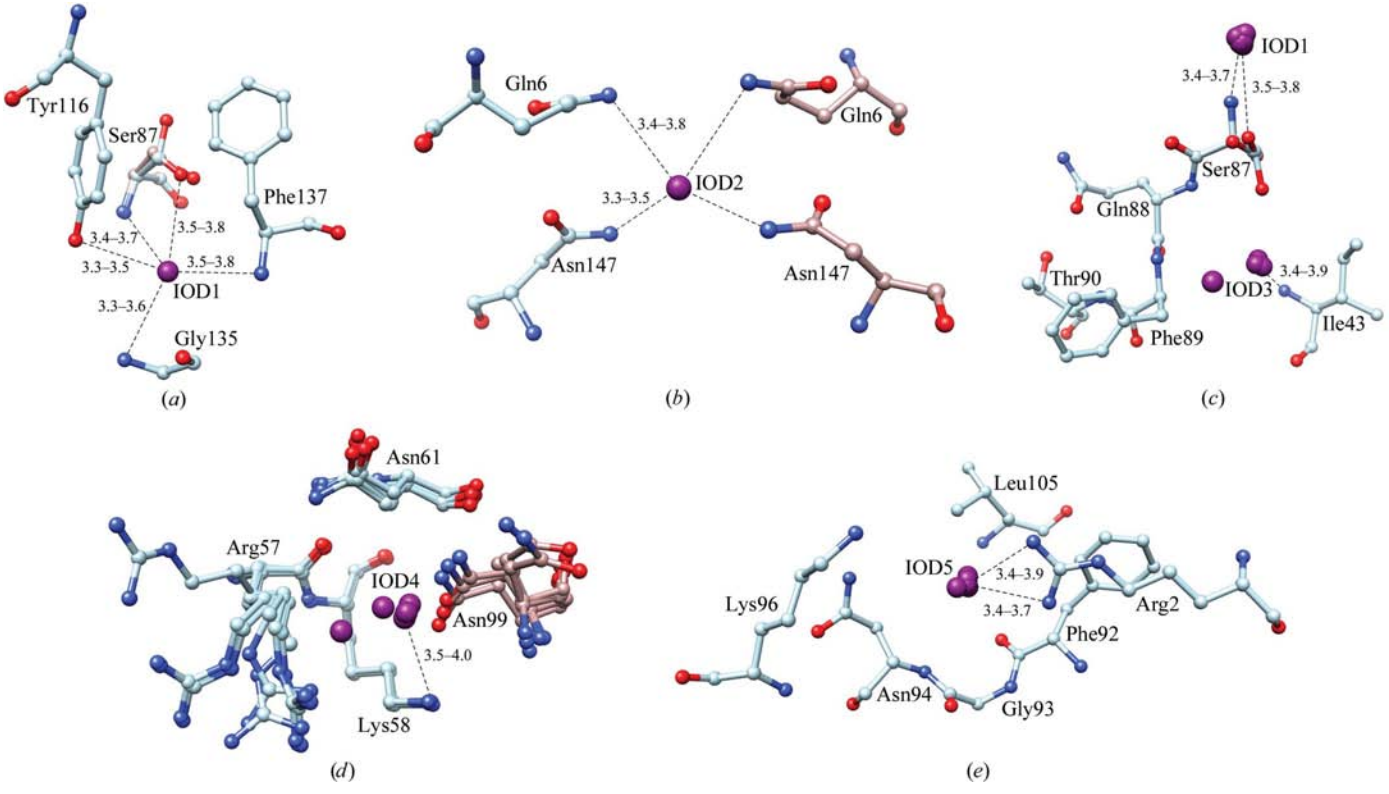

Figure 5
The five conserved iodide-binding sites in molecules *A*–*F* of the PfDTD-*P*1 structure. (*a*) IOD1 at the bottom of the active-site cavity, (*b*) IOD2 at the twofold-related dimer interface, (*c*) IOD3 near the active site, (*d*) IOD4 near Lys58 and (*e*) IOD5 near Arg2. The reference molecule and its twofold-related dimeric partners are shown in blue and brown, respectively, and bound iodides are shown as magenta spheres. The interactions are shown by dashed lines and distances are in Å.

± 6, $\beta = 101 \pm 5$, $\gamma = 86 \pm 14^{\circ}$. A large variation in the *a* or *b* unit-cell parameter and γ angle was observed for the T1, T2 and T4 forms. In all *P*1 forms (T1–T5) the dimers *AB*, *CD* and *EF* are essentially identical, with structural polymorphism found mostly in the insertion residues (IL) and in the two long loops L1 and L2 (Fig. 3*a*). The insertion residues are ordered in a few of the PfDTD packing environments. The crystal packing of the T1–T5 forms shows that the dimer arrangement is identical in the unit cell but that the dimers differ in the manner in which they are orientated in the unit cell (Fig. 7*a*). The *CD* dimers of the T1 and T2 forms are orientated at 2° and 4.7° along the *a* axis and are translated by 5.9 and 0.2 Å along the *a* axis with respect to the T3 form. The large translation distance correlates with the ∼5 Å enlargement in the *a* axis of the T1 form. The dimer orientation angles (2–5°) in the T1 and T2 forms are also correlated with the enlargement in the γ angle (∼4–5°). In the T4 and T5 forms the arrangement of the dimers is identical but they are reoriented

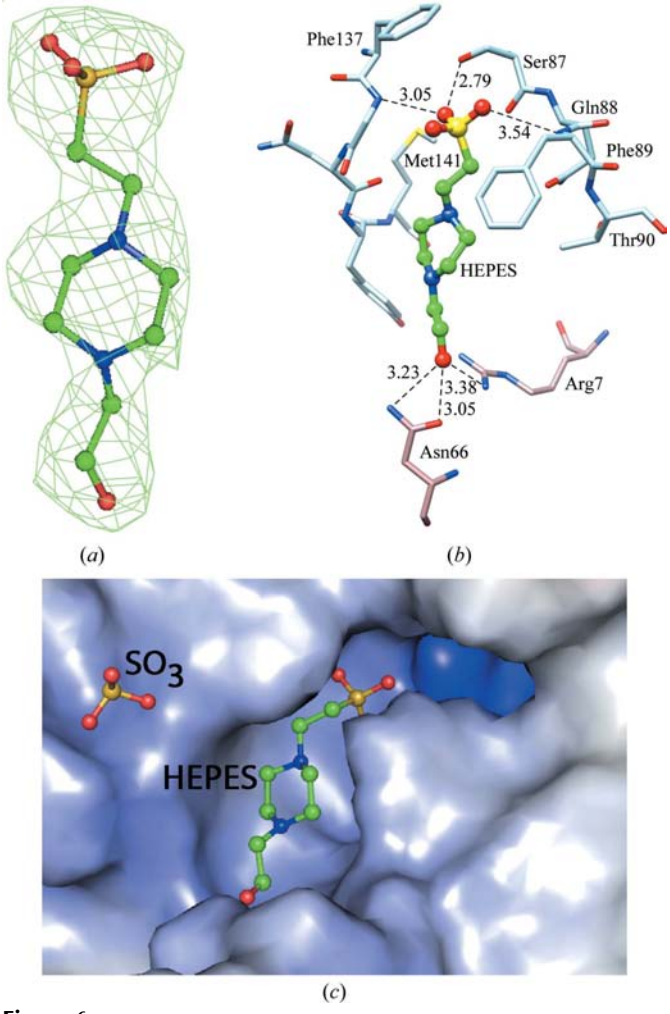

Figure 6
Bound HEPES and SO_3 molecules in the PfDTD-HEPES structure. (*a*) The difference electron-density map of bound HEPES prior to inclusion in the refinement model (contoured at the 2.0σ level). (*b*) Bound HEPES near the active site of molecule *D*. HEPES is shown in green, with hydrogen bonds shown as dashed lines. Reference molecule *D* is shown in blue and its twofold-related dimeric partner molecule *C* is shown in brown. (*c*) Electrostatic surface representation of the PfDTD active site along with bound HEPES and SO_3 molecules. The electrostatic surface is displayed as a colour gradient from red (electronegative, $\leq -10\ kTe^{-1}$) to blue (electropositive, $\geq 10\ kTe^{-1}$).

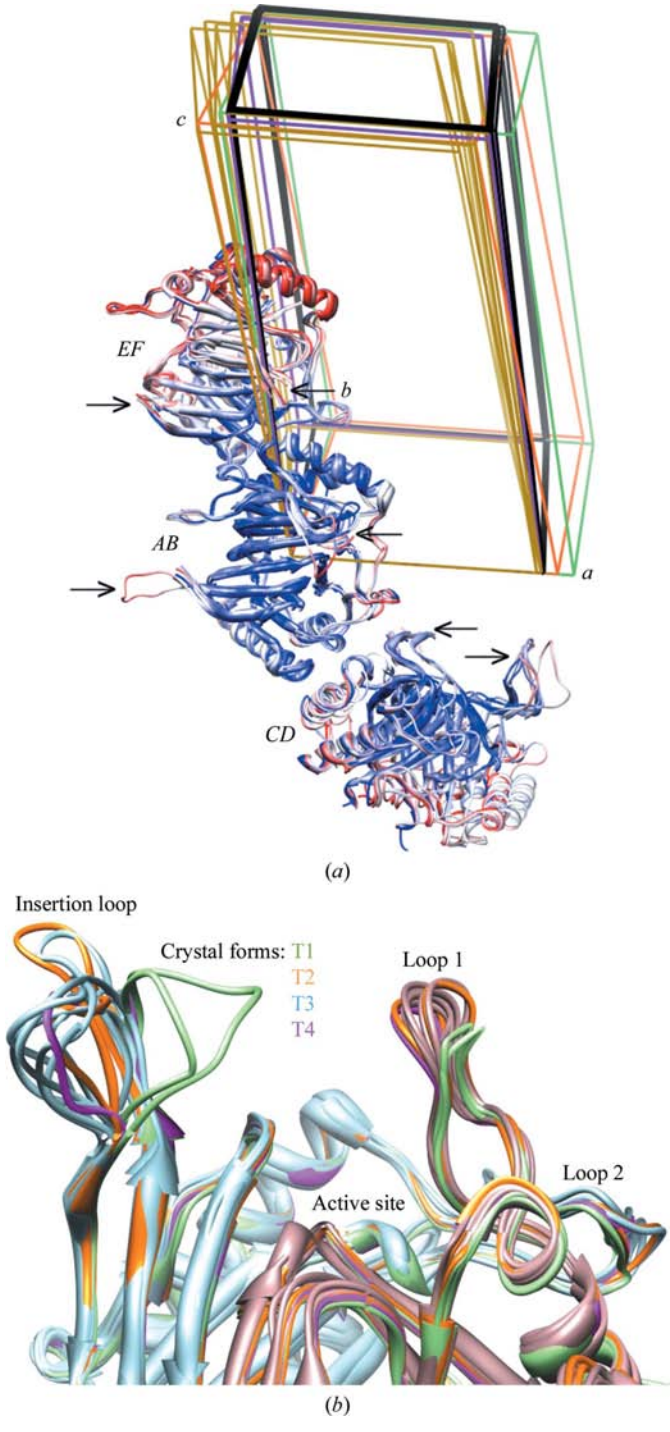

Figure 7
Variation in crystal packing and insertion-loop residue conformations. (*a*) The different (T1–T3) forms of triclinic crystal packing of PfDTD; the molecules are rendered by *B*-factor variation. For clarity, the molecules of the T4 and T5 forms are not included. Unit cells are shown in green, orange, black, brown and violet for the T1, T2, T3, T4 and T5 forms, respectively. The insertion loop is indicated by an arrow. (*b*) A view of various conformations of the insertion residues (17–26). These residues were disordered in most of the T4 and T5 forms.

Table 4
Polymorphic and non-isomorphic morphology of PfDTD crystals.

Data set†	Unit-cell parameters (Å, °)	No. of ordered insertion-loop residues‡	Resolution (Å)	Condition§	Shape
Triclinic space group *P*1					
T1	$a = 59, b = 55, c = 93, \alpha = 106, \beta = 103, \gamma = 99$	3	3.30	MES1	Plate$^{\text{Native}}$
T2	$a = 55, b = 58, c = 92, \alpha = 102, \beta = 105, \gamma = 100$	2	2.74	MES1	Plate$^{\text{I-SAD}}$
T3	$a = 52, b = 55, c = 93, \alpha = 107, \beta = 102, \gamma = 94$		3.00	MES1	Plate
T3	$a = 53, b = 55, c = 93, \alpha = 107, \beta = 101, \gamma = 95$	1	2.82	MES1	Plate
T3	$a = 52, b = 55, c = 93, \alpha = 107, \beta = 102, \gamma = 95$	1	2.91	PEG 1500	Plate
T3	$a = 52, b = 55, c = 93, \alpha = 107, \beta = 102, \gamma = 94$	1	3.00	MES1	Plate
T3	$a = 52, b = 55, c = 93, \alpha = 107, \beta = 102, \gamma = 95$	1	2.75	PEG 1500	Plate
T4	$a = 52, b = 53, c = 91, \alpha = 105, \beta = 104, \gamma = 86$¶	2	2.21	PEG 1500	Block
T4	$a = 52, b = 53, c = 90, \alpha = 105, \beta = 106, \gamma = 86$††	—	2.83	HEPES	Plate
T4	$a = 52, b = 53, c = 92, \alpha = 108, \beta = 102, \gamma = 89$‡‡	—	2.80	MES1	Block
T4	$a = 51, b = 53, c = 90, \alpha = 107, \beta = 103, \gamma = 88$§§	—	2.70	MES1	Plate
T5	$a = 52, b = 54, c = 91, \alpha = 106, \beta = 102, \gamma = 91$	—	3.00	MES1	Plate
T5	$a = 52, b = 53, c = 91, \alpha = 106, \beta = 102, \gamma = 91$	—	2.10	MES1	Plate
Monoclinic, space group $P2_1$					
M1	$a = 77$–$79, b = 93$–$95, c = 130$–$132, \beta = 106$–107	1	3.3	MES2	Block
M2	$a = 47$–$48, b = 76$–$79, c = 128$–$132, \beta = 95$–98	1	2.4	MES2	Block
M3	$a = 47.58, b = 78.72, c = 260.76, \beta = 96$–$102$	2	2.9	MES2	Block
Tetragonal, space group $P4_3$					
TG	$a = b = 76$–$77, c = 214$-216	—	3.3	PEG 1500	Pyramid

† We collected more than 30 data sets for triclinic forms (T1–T5) and 15 data sets for the monoclinic (M1, M2 and M3) and tetragonal (TG) forms. ‡ Electron density for insertion residues (17–26) is observed and these residues adopt different conformations as shown in Fig. 7(*b*). § Crystallization conditions: MES1, 0.1 *M* MES pH 6.2–6.5, 25% PEG 3350; MES2, 0.1 *M* MES pH 6.8, 25–30% PEG 3350; HEPES, 0.1 *M* Tris–HEPES pH 7.5–8.5, 25–30% PEG 3350; PEG 1500, 25% PEG 1500. ¶ For comparison, for T4 we reindexed the data from *h*, *k*, *l* to −*h*, −*k*, *l*. The corresponding deposited unit-cell parameters are as follows: $a = 52, b = 53, c = 91$ Å, $\alpha = 75, \beta = 76, \gamma = 86°$. †† $a = 52, b = 53, c = 90$ Å, $\alpha = 75, \beta = 74, \gamma = 86°$. ‡‡ $a = 52, b = 53, c = 92$ Å, $\alpha = 72, \beta = 78, \gamma = 89°$. §§ $a = 51, b = 53, c = 90$ Å, $\alpha = 73, \beta = 77, \gamma = 88°$.

by 5–10° together with a translation of 0.5–3.0 Å along the rotation axis with respect to the T1–T3 forms.

Analysis of the packing in all *P*1 space-group forms of PfDTD indicates variable packing environments for the dimers and variable insertion-residue conformations (Fig. 7*b*). This structural plasticity is summarized in Fig. 7 and we feel that the non-isomorphism witnessed in *P*1 crystals of PfDTD may be a consequence of the inherent flexibility of the ten insertion residues, which happen to be specific to the malaria-parasite enzyme. The functional significance of this 'flexible-loop' addition in DTD remains unclear, but our present report clearly shows that it is possible to detail at least a few conformations of such insertions in protein sequences.

The X-ray facility at ICGEB is funded by the Wellcome Trust, UK. MY and SK were supported by an FP7 grant from EU grants PREMALSTRUCT and MEPHITIS, respectively. TKB and AS were supported by grants from the Department of Biotechnology, Government of India.

References

Adams, P. D., Grosse-Kunstleve, R. W., Hung, L.-W., Ioerger, T. R., McCoy, A. J., Moriarty, N. W., Read, R. J., Sacchettini, J. C., Sauter, N. K. & Terwilliger, T. C. (2002). *Acta Cryst.* D**58**, 1948–1954.

Brodersen, D. E., Clemons, W. M., Carter, A. P., Wimberly, B. T. & Ramakrishnan, V. (2003). *Acta Cryst.* D**59**, 2044–2050.

Chen, V. B., Arendall, W. B., Headd, J. J., Keedy, D. A., Immormino, R. M., Kapral, G. J., Murray, L. W., Richardson, J. S. & Richardson, D. C. (2010). *Acta Cryst.* D**66**, 12–21.

Cohen, G. E. (1997). *J. Appl. Cryst.* **30**, 1160–1161.

Dauter, Z., Dauter, M. & Rajashankar, K. R. (2000). *Acta Cryst.* D**56**, 232–237.

Emsley, P. & Cowtan, K. (2004). *Acta Cryst.* D**60**, 2126–2132.

Ferri-Fioni, M. L., Schmitt, E., Soutourina, J., Plateau, P., Mechulam, Y. & Blanquet, S. (2001). *J. Biol. Chem.* **276**, 47285–47290.

Kemp, M., Bae, B., Yu, J. P., Ghosh, M., Leffak, M. & Nair, S. K. (2007). *J. Biol. Chem.* **282**, 10441–10448.

Laskowski, R. A., MacArthur, M. W., Moss, D. S. & Thornton, J. M. (1993). *J. Appl. Cryst.* **26**, 283–291.

Lim, K., Tempczyk, A., Bonander, N., Toedt, J., Howard, A., Eisenstein, E. & Herzberg, O. (2003). *J. Biol. Chem.* **278**, 13496–13502.

Murshudov, G. N., Vagin, A. A. & Dodson, E. J. (1997). *Acta Cryst.* D**53**, 240–255.

Otwinowski, Z. & Minor, W. (1997). *Methods Enzymol.* **276**, 307–326.

Pape, T. & Schneider, T. R. (2004). *J. Appl. Cryst.* **37**, 843–844.

Perrakis, A., Harkiolaki, M., Wilson, K. S. & Lamzin, V. S. (2001). *Acta Cryst.* D**57**, 1445–1450.

Pettersen, E. F., Goddard, T. D., Huang, C. C., Couch, G. S., Greenblatt, D. M., Meng, E. C. & Ferrin, T. E. (2004). *J. Comput. Chem.* **25**, 1605–1612.

Randal, M. & Kossiakoff, A. A. (2000). *Acta Cryst.* D**56**, 14–24.

Redinbo, M. R., Stewart, L., Champoux, J. J. & Hol, W. G. J. (1999). *J. Mol. Biol.* **292**, 685–696.

Sheldrick, G. M. (2008). *Acta Cryst.* A**64**, 112–122.

Sheldrick, G. M., Hauptman, H. A., Weeks, C. M., Miller, R. & Usón, I. (2001). *International Tables for Crystallography*, Vol. *F*, edited by M. G. Rossmann & E. Arnold, ch. 16, pp. 333–345. Dordrecht: Kluwer Academic Publishers.

Swarnamukhi, P. L., Sharma, S. K., Padala, P., Surolia, N., Surolia, A. & Suguna, K. (2007). *Acta Cryst.* D**63**, 458–464.

Vagin, A. & Teplyakov, A. (1997). *J. Appl. Cryst.* **30**, 1022–1025.

Verschueren, K. H. G., Tyrrell, R., Murshudov, G. N., Dodson, E. J. & Wilkinson, A. J. (1999). *Acta Cryst.* D**55**, 369–378.

Yogavel, M., Gill, J., Mishra, P. C. & Sharma, A. (2007). *Acta Cryst.* D**63**, 931–934.

Yogavel, M., Gill, J. & Sharma, A. (2009). *Acta Cryst.* D**65**, 618–622.

Zhang, X. J., Wozniak, J. A. & Matthews, B. W. (1995). *J. Mol. Biol.* **250**, 527–552.